Parameter Characterization of Low Frequency Pulsating Emissions from Space Vector PWM drives

Mathias Enohnyaket, Kalevi Hyyppä, and Jerker Delsing
EISLAB
Luleå University of Technology
SE-97176 Luleå Sweden
Email: Mathias.Enohnyaket@ltu.se, Kalevi.Hyyppa@ltu.se,
Jerker.Delsing@ltu.se

***Abstract*—Power converters in hybrid electric drives constitute a major source of electromagnetic disturbances. Recent studies have established that the space vector PWM scheme commonly employed in drive systems, generates low frequency pulsating (LFP) emissions, at a frequency of $6f_0$, where f_0 is the fundamental frequency the phase voltages. The switching of voltage vectors generates common mode current (i_{cm}) spikes due to the presence of stray capacitances and inductances. Across sector boundaries, the i_{cm} spikes superpose forming spikes of double or tipple amplitude which constitute the LFP emissions. These pulsating emissions could pose EMC issues, and functionality issues like torque pulsations and speed fluctuations that could affect the reliability of the drive. This paper investigates the effects of drive speed, load, and converter slew rates, on the amplitude of the LFP emissions, using theoretical models.**

Keywords: Low frequency pulsating emissions, EMI, torque pulsations, common mode currents, time domain measurements, drive system.

I. Introduction

The increasing demand for clean energy systems in vehicles has propelled a rapid development of electric and hybrid electric vehicles (HEV). Power converters play a central role in hybrid electric drive systems and constitute a major source of electromagnetic disturbances. PWM switching of DC/AC converters generates common mode current spikes (i_{cm}) due to the presence of stray capacitances. These spikes account for the emissions from PWM drives at harmonics of the switching frequency (f_c) and harmonics of the fundamental frequency f_0, mostly reported in the literature [1]–[8].

Amongst the PWM schemes, the space vector scheme is mostly preferred for its flexible speed control capabilities [9]–[12]. However recent studies have reported some issues related to the space vector scheme. In [8], it was shown that the amplitude of current ripples at switching frequency (f_c) are influenced by the placement of active vectors within each half carrier or PWM period. Issues related to the crossing of sector boundaries in the space vector hexagon has been reported [1], [13]–[15]. In [14], the formation of common mode current spikes due to sector boundary crossing was mentioned. In [13], the generation of large torque pulsations due to sector boundary crossing was reported. The generation of low frequency pulsating (LFP) common mode emissions during sector boundary crossing reported in [15], shall be considered in this paper. The LFP emissions were formed by the superposition of common mode current spikes generated during the switching of voltage vectors. In the space vector PWM scheme, a given reference vector is obtained as a linear combination of the adjacent voltage vectors ($\mathbf{V}_k$, $\mathbf{V}_{k+1}$), with duty cycles D_k and D_{k+1}, respectively [9], [10]. The duty cycles determine the time interval between the i_{cm} spikes. Closed to sector boundaries, either D_k or D_{k+1} tends to zero causing a superposition of i_{cm} spikes to occur. These pulsations enhance emissions at harmonics of switching frequency (f_c); create low frequency magnetic fields, and when injected into electric motors could lead to torque pulsations and speed fluctuations [13], [14], [16], [17]. This paper investigates the effects of drive speed, load, and converter slew rates, on the amplitudes of the LFP emissions, using theoretical models.

Section II presents some measurements from an HEV showing LFP emissions. Section III presents the theoretical modeling of LFP emissions using Gaussian pulses, and models the effects of different drive parameters. Section V rounds off with some discussions and conclusions.

II. Measurements on HEV

This section presents some measurements from an HEV showing LFP emissions.

978-1-4244-8218-4/10/$26.00 ©2010 IEEE

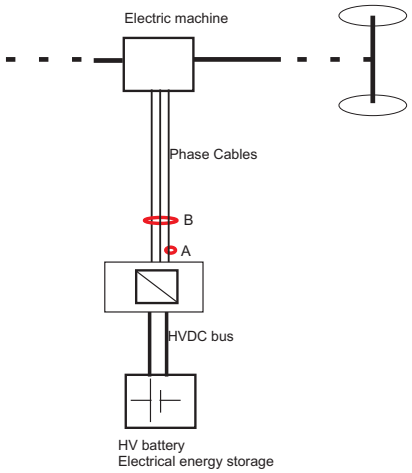

Fig. 1. Hybrid Drive System on which measurements were performed.

A. Measurement setup

Fig. 1 shows a schematic of the hybrid drive system on which the measurements were performed. The electric machine is a three phase synchronous machine. The phase current was measured at location A, with a Tektronix current probe (model TCP404XL), of bandwidth dc to 2 MHz, and peak current 750 A DC. Common mode currents were measured at location B, with a Powertek Rogowski coil (model CWT 6B) of bandwidth 0.1 Hz to 16 MHz, with peak current rating of 1.2 kA, and 8 $kA/\mu s$. The measurements were recorded on a Tektronix digital oscilloscope (TDS7254), of bandwidth 2.5 GHz, and maximum sampling rate of 20 giga samples per second.

B. Some results

The measurements were performed under different driving modes, with the current probes located at the positions A and B on the drive train, as shown in Fig. 1. Measurements from two different cases are presented. The objective of case I was to capture the events occurring during switching. A short interval of about five PWM switching cycles was considered. In order to capture the events in detail, a high oscilloscope sampling rate of 250 megasamples per second, was used. Results from case I, shown in Fig. 2, show superposition of i_{cm} switching spikes. In Case II, the amplitude of the phase current is slowly decreased from about 250 A down to 50 A, with a phase current frequency of about 50 Hz. This case is presented in Fig. 3. Low frequency pulsating (LFP) emissions with periodicity of about 0.008 s in the common mode currents are observed.

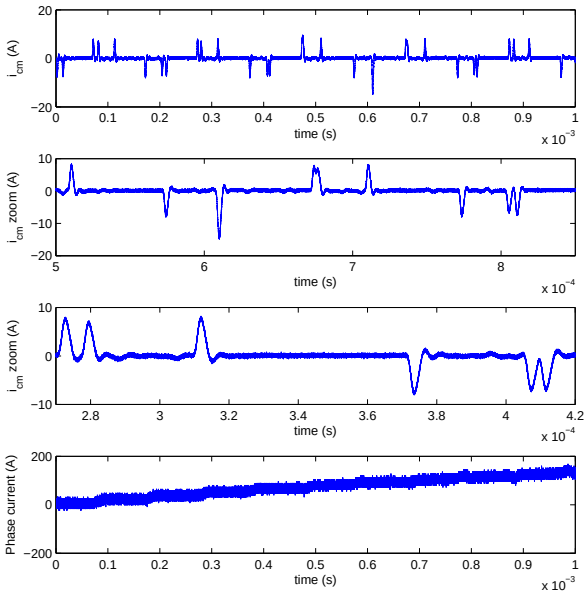

Fig. 2. Case I showing the superposition of i_{cm} spikes during switching. The top plot is the i_{cm} currents. The second subplot is obtained by zooming in the region 0.50 s to 0.85 s of the top plot. The third subplot is obtained by zooming in the region 0.250 s to 0.42 ms of the top plot. The bottom subplot is the phase current. Oscilloscope sampling rate is 250 mega samples per second, which is 400 times Nyquist sampling frequency.

III. Theoretical Modeling

Representing an i_{cm} spike as a Gaussian pulse, the spike pattern for different PWM schemes can be reconstructed by superposition [18], [19]. The pattern generated by the space vector PWM (SV-PWM) scheme is considered, since it is the scheme used in the drive train on which the measurements were performed. This section briefly presents the space vector scheme and models effects of drive speed, load, and converter slew rates, on the amplitude of the LFP emissions.

A. Space Vector PWM (SV-PWM) scheme

The space vector hexagon shown in Fig. 4 represents the classical SV-PWM scheme [9]–[12]. An arbitrary reference voltage vector ($\boldsymbol{V}_{ref}$) defined in (1) can be represented as a linear combination of two adjacent voltage vectors ($\boldsymbol{V}_k$ and $\boldsymbol{V}_{k+1}$), and zero vectors ($\boldsymbol{V}_0$ and $\boldsymbol{V}_7$), as described in (2),

$$\boldsymbol{V}_{ref} = V_{ds}\hat{\mathbf{d}} + V_{qs}\hat{\mathbf{q}} \tag{1}$$

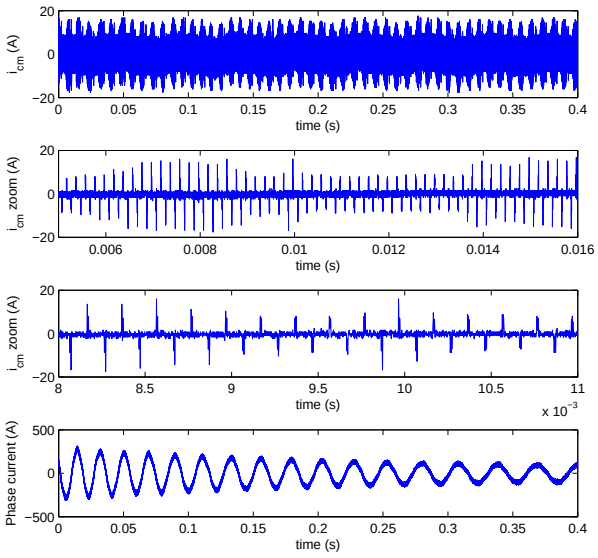

Fig. 3. Case II showing LFP emissions with periodicity 0.008 s. The second subplot is obtained by zooming in the region 0.005 s to 0.016 s of the top plot. The third subplot is obtained by zooming in the region 0.008 s to 0.011 s of the top plot. The bottom plot is the phase current. Oscilloscope sampling rate is 1.25 mega samples per second, which is twice the Nyquist frequency.

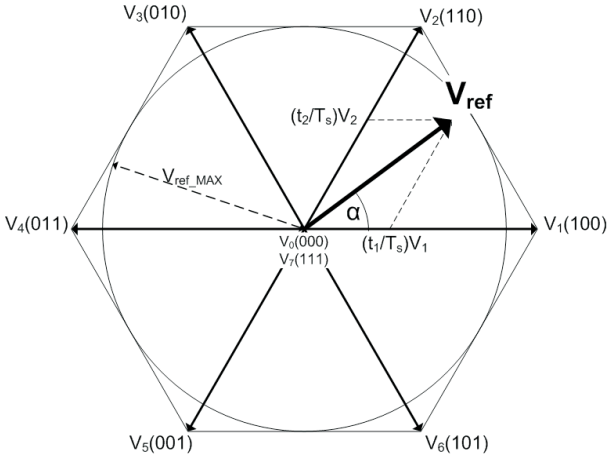

Fig. 4. Space vector scheme showing voltage vectors $V_0, V_1, ..., V_7$ and arbitrary reference voltage vector $\boldsymbol{V}_{ref}$. The binary numbers $000, 001, ...$ represents the switch states.

$$\boldsymbol{V}_{ref} = D_k\boldsymbol{V}_k + D_{k+1}\boldsymbol{V}_{k+1} + [1-(D_k+D_{k+1})]\boldsymbol{V}_{0,7} \tag{2}$$

where $D_k = \frac{T_k}{T_s}$ is the duty cycle, T_k is the time spent on the $\boldsymbol{V}_k$ voltage vector, T_s the PWM period, and V_d is the dc source voltage. The voltage vectors $\boldsymbol{V}_k$ are defined as

$$\boldsymbol{V}_k = \frac{2}{3}\, V_d\, \exp j\frac{\pi(k-1)}{3}. \tag{3}$$

For half a PWM period, D_k is constrained as

$$D_k + D_{k+1} + D_{0,7} = 0.5, \tag{4}$$

where $D_{0,7}$ is the duty ratio for either $\boldsymbol{V}_0$ or $\boldsymbol{V}_7$ zero voltage vectors. Considering that $\boldsymbol{V}_{0,7} = 0$, $\boldsymbol{V}_{ref}$ is simplified as

$$\boldsymbol{V}_{ref} = D_k\boldsymbol{V}_k + D_{k+1}\boldsymbol{V}_{k+1}. \tag{5}$$

Using (1) to (5), the switching times T_k and T_{k+1} are obtained. The $T_k's$ determine when the converter switches fire or voltage transitions occur. This, in turn, determines the interval between the i_{cm} spikes.

B. Modeling of i_{cm} spikes

The spike rise time and amplitude are varied using parameters A and C, as shown in Fig. 5. The time of occurrence of the spike is varied by moving the centre of the Gaussian pulse, and is equivalent to varying parameter b in (6).

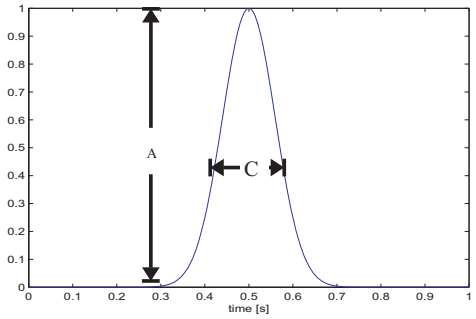

Fig. 5. Gaussian pulse of height A, width C and centered at time $t = 0.5s$. The center of the pulse corresponds to the parameter b in (6).

$$f(t) = A\, \exp\left(\frac{-(t-b)^2}{2C^2}\right), \tag{6}$$

Consider a V_{ref} in the sector 1, where $0 < \alpha < \frac{\pi}{3}$.
In the symmetric SV-PWM scheme [11], a feasible PWM switching cycle is the following:
$\{...000 \rightarrow 100 \rightarrow 110 \rightarrow 111$
$\rightarrow 111 \rightarrow 110 \rightarrow 100 \rightarrow 000...\}$,
with switching times $\{\frac{D_1}{2}, \frac{D_2}{2}, \frac{D_7}{2}, \frac{D_7}{2}, \frac{D_2}{2}, \frac{D_1}{2}\}$, respectively. The i_{cm} spike pattern generated by this switching cycle is shown in Fig. 6.

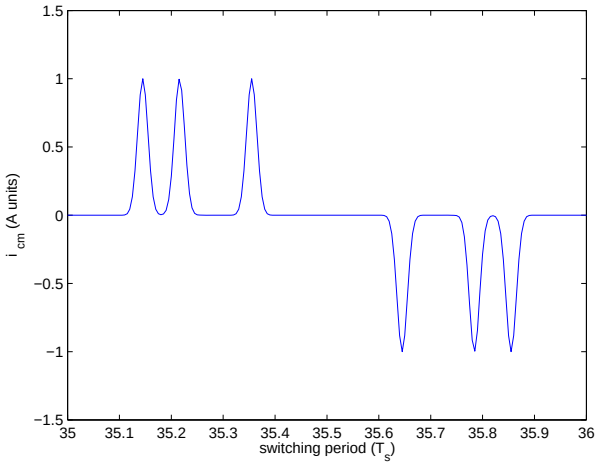

Fig. 6. i_{cm} pattern for one PWM cycle, with $\boldsymbol{V}_{ref}$ in sector 1. $time$ is expressed in terms of PWM switching periods, $T_s = 0.0002s$

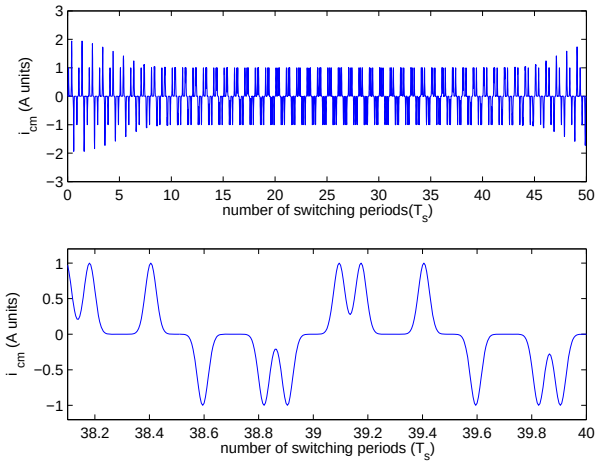

Fig. 7. Simulation results showing LFP emissions of periodicity 0.001 s. The results obtained using the following parameter settings: $0 < D_k \leq 0.2$, $T_s = 0.0002s$, $T_0 = 50T_s$. The lower subplot is obtained by zooming in the response when $38.1T_s \leq time \leq 40.0T_s$. This corresponds to case I, presented in Fig. 2 showing the superposition of switching spikes.

C. Reconstruction of LFP emissions

An anticlockwise rotation of a constant amplitude reference voltage $\mathbf{V}_{ref}$ generates steady state sinusoidal phase voltages. This is obtained by varying D_k and D_{k+1} while respecting the constraints given in (4). Closed to sector boundaries, either D_k or D_{k+1} tends to zero. These cause spike superpositions during sector boundary crossings, forming double or tripple amplitude spikes which constitute the LFP emissions. The six sector boundaries give rise to six LFP pulses in one complete revolution.

$$T_0 = 6\,T_{LFP} \tag{7}$$

The period of the sinusoidal phase voltage T_0, is thus related to the period of the LFP emissions (T_{LFP}) as in (7). Fig. 7 shows simulated LFP emissions of periodicity 0.001 s. The results were obtained using the following parameter settings: $0 < D_k \leq 0.2$, $T_s = 0.0002s$, $T_0 = 50T_s$. Fig. 8 presents simulation results showing LFP emissions of periodicity $T_{LFP} = 40T_s = 0.008s$, obtained using the following parameter settings: $0 < D_k \leq 0.45$, $T_s = 0.0002s$, $T_0 = 240T_s$. This was a reconstruction attempt of case II, shown in Fig. 3.

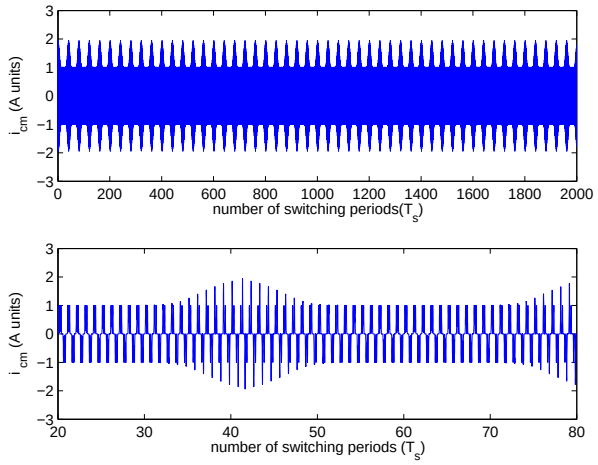

Fig. 8. Simulation results showing LFP emissions of $40T_s = 0.008s$. The results obtained using the following parameter settings: $0 < D_k \leq 0.2$, $T_s = 0.0002s$, $T_0 = 240T_s$. This a reconstruction of case II, shown in Fig. 3. The lower subplot is obtained by zooming in the response when $20T_s \leq time \leq 80T_s$.

IV. Parameters affecting the LFP emissions

In this section, the dependence of the amplitudes of the LFP emissions on the voltage slew rates of the converter switches, the drive speed, and load is investigated using the theoretical models developed in section III.

A. Effects of Voltage slew rates on LFP emissions

Close to the boundary between the kth sector, and the $(k+1)$th sector, D_k becomes comparable to the width of the gaussian pulse (C), as described in (8). The rise time t_r is an estimate of the voltage slew rate, for a fixed dc source voltage, and is approximately equal to the pulse width (C) of the generated common mode current spike [2]. In the boundary region, marked by θ in Fig. 9, D_k can be represented as a fraction of the maximum duty cycle D_kmax, as in (8) and (9), assuming that PWM

period $T_s = 1$. When $D_k = C$, the angular width of the LFP emissions, $\theta = \theta_c$ can expressed as a fraction of the sector angle as in (10). Using (8) to (10), the expression for θ_c in terms of t_r and $D_k max$ given in (11), is obtained. The width of the LFP emissions in seconds is obtained as $d_{LFP} = \theta_c/2\pi * T_0$ and is given in (12).

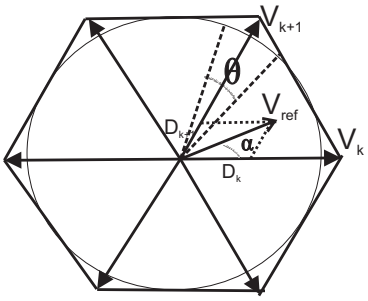

Fig. 9. Space vector hexagon showing the boundary region, where $D_k \leq C \sim t_r$, denoted by θ

$$D_k \leq C \sim t_r, D_k T_s = C \tag{8}$$

$$D_k = \frac{D_k max}{x} \tag{9}$$

$$\theta_c/2 = \frac{\pi}{3}/x \tag{10}$$

$$\theta_c/2 = \frac{\pi}{3}\frac{t_r}{D_k max} \tag{11}$$

$$d_{LFP} = \frac{1}{6}\frac{1}{D_k max}\frac{T_0}{T_s}t_r \tag{12}$$

$$d_{LFP} \propto t_r \tag{13}$$

The effects of slew rates is described by (13) when $D_k max$, T_0, and T_s are held constant. Thus the larger the rise time, the larger the width of the LFP emissions. This is shown in Fig. 10 and Fig. 11, where $C \sim t_r = 0.02s$ and $C \sim t_r = 0.035s$, respectively.

B. Effects of drive speed on LFP emissions

The drive speed is assumed proportional to the fundamental frequency of the phase voltages ($1/T_0$). From (11), when θ_c is fixed, d_{LFP} is given by

$$d_{LFP} = \frac{\theta_c}{2\pi}T_0. \tag{14}$$

This is seen in the simulated prediction of LFP emissions when $T_0 = 0.6s$, shown in Fig. 10, with $d_{LFP} \sim 100T_s$.

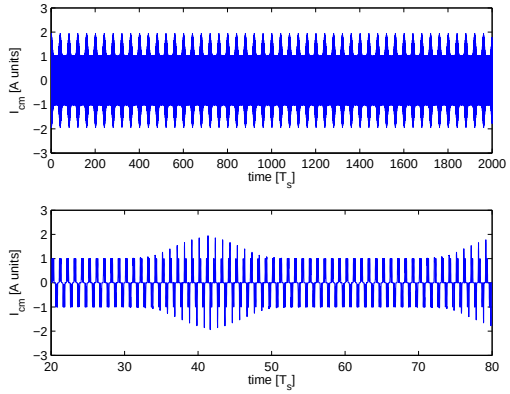

Fig. 10. Reconstruction of case II with $C \sim t_r = 0.02s$,$d_{LFP} \sim 10T_s$, $T_{LFP} = 40T_s = 0.008s$ and $T_0 = 240T_s$. Parameter settings: $0 < D_k \leq 0.45$, $T_s = 0.0002s$. The lower subplot is a zoom of the region $20T_s < t < 80T_s$.

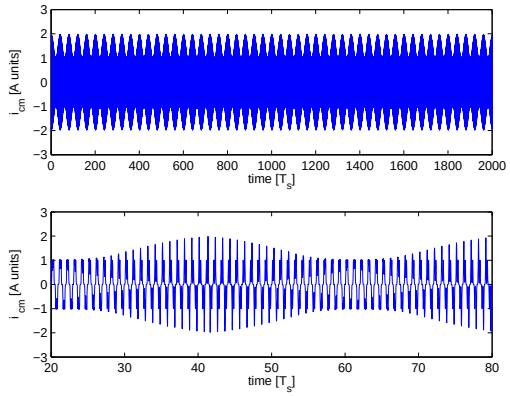

Fig. 11. Reconstruction of case II with $C \sim t_r = 0.035s$, $d_{LFP} \sim 20T_s$, $T_{LFP} = 40T_s = 0.008s$ and $T_0 = 240T_s$. Parameter settings: $0 < D_k \leq 0.45$, $T_s = 0.0002s$.

C. Effects of load on LFP emissions

The load or torque output is assumed proportional to the amplitude of the phase current. This is simulated by varying the maximum duty cycle $D_k max$ in the interval $0 < D_k max < 0.5$. From (12) it is observed that d_{LFP} is proportional to $D_k max$, when T_0, t_r and T_s are held constant. This is an indication of light load instabilities. This is shown in Fig. 13, when $D_k max = 0.05$. It is observed that the LFP pulses overlap in this case, unlike in the previous cases where was set to 0.2 or 0.45.

V. Discussions and Conclusions

Drive systems employing the space vector PWM scheme could emit Low Frequency Pulsating (LFP) emissions at a frequency of $6f_0$, where f_0 is the fundamental frequency of the phase voltages. The LFP emis-

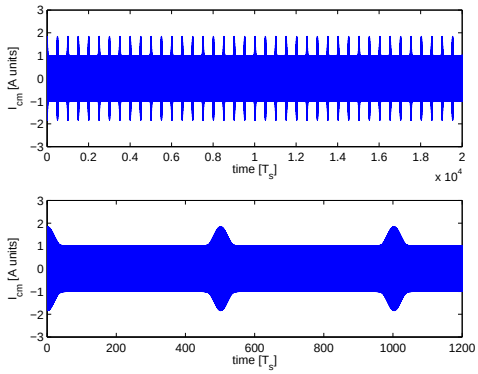

Fig. 12. Simulated prediction of LFP emissions with $T_0 = 3000T_s = 0.6s$ and $d_{LFP} \sim 100T_s$. Parameter settings: $0 < D_k \leq 0.45$, $T_s = 0.0002s$. The lower subplot is a zoom of the region $0 < t < 1200T_s$

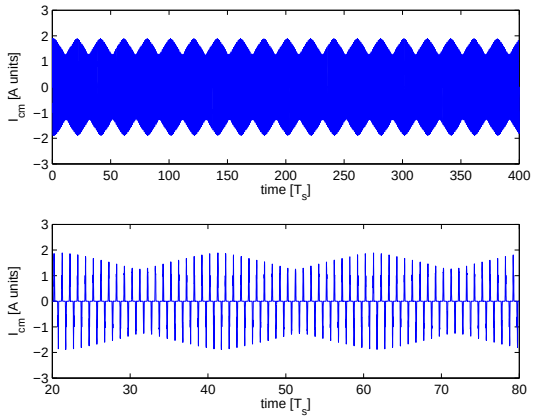

Fig. 13. Light load conditions, with a period of 0.005 s. Parameter settings: $0 < D_k \leq 0.05$, $T_s = 0.0002s$, $T_0 = 150T_s$. The lower subplot is a zoom of the region $20T_s < t < 80T_s$.

sions is built up from double or tipple amplitude common mode current spikes, formed from the superposition of common mode spikes generated during sector boundary crossings. Measurements from an HEV showing the LFP emissions were presented. Using simple theoretical models the effects of parameters like the voltage slew rates, drive speed and drive load on the LFP emissions of have been investigated. The coupling of these pulsations to torque pulsations requires further investigations, however, relationships between current harmonics and torque pulsations have been deveped in [16], [17]. Mitigation approaches shall be investigated in a future work.

REFERENCES

[1] Q. Liu, "Modular approach for characterizing and modeling conducted EMI emissions in power converters," Ph.D. dissertation, Virginia Polytechnic Institute and State University, VA, USA, 2005.

[2] C. Paul, *Introduction to Electromagnetic Compatibility*. John Wiley and Sons, Inc., New York, 2006.

[3] T. Hubing, "Using component level measurements to determine system level radiated emissions," in *Proc. of the IEEE Int. symposium on EMC*, Detroite MI, USA, 2008.

[4] Q. Liu, F. Wang, and D. Boroyevich, "Frequency-domain EMI noise emission characterization of switching power modules in converter systems," in *Proc. of IEEE Applied Power Electronics Conference and Exposition*, 2005, pp. 787–79.

[5] R. Thomas, F. Li, and C. Garrett, "Prediction of radiated EMI from high frequency power converters," in *Proc. of IEE international Conference on Power Electronics and Variable Speed Drives*, 2000, pp. 80–85.

[6] K. Mainali, R. Oruganti, K. Viswanathan, and N. Swee, "A metric for evaluating the EMI spectra of power converters," *IEEE Trans. Power Electron.*, vol. 23, no. 4, pp. 2075–2081, 2008.

[7] N. Mutoh, J. Nakashima, and M. Kanesaki, "Multilayer power printed structures suitable for controlling EMI noises generated in power converters," *IEEE Trans. Power Electron.*, vol. 50, no. 6, pp. 1085–1094, 2003.

[8] D. G. Holmes, "The significance of zero space vector placement for carrier-based pwm schemes," *IEEE Trans. Ind. Applicat.*, vol. 32, no. 5, pp. 1122 – 1129, 1996.

[9] M. Ehsani, S. Gay, and A. Amadi, *Modern Electric, Hybrid Electric, and Fuel Cell Vehicles*. CRC Press, New York, 2005.

[10] G. Oritiand, A. L. Julian, and A. Lipo, "A new space vector modulation strategy for common mode voltage reduction," in *Proc. of the IEEE PESC'97*, Saint Louis, MO, USA, 1997, pp. 1541 – 1546.

[11] M. M. Bech, "Random pulse-width modulation techniques for power electronic converters," Ph.D. dissertation, Aalborg University, Aaborg, Denmark, 2000.

[12] I. Husain, *Electric and Hybrid Vehicles*. CRC Press, New York, 2003.

[13] K. Basu, J. Prasad, G. Narayanan, H. Krishnamurthy, and R. Ayyanar, "Reduction of torque ripple in induction motor drives using an advanced hybrid pwm technique," *IEEE Trans. Ind. Applicat.*, vol. 00, no. 99, pp. 1–1, 2009.

[14] M. Cirrincione, M. Pucci, G. Vitale, and G. Cirrincione, "A new direct torque control strategy for the minimization of common-mode emissions," *IEEE Trans. Ind. Applicat.*, vol. 46, no. 2, pp. 504 – 517, 2006.

[15] M. Enohnyaket, K. Hyyppa, and J. Delsing, "Generation of low frequency pulsating emissions from PWM power converters," IEEE Power Electronics Society Newsletter, Submitted 2010.

[16] J. Song-Manguelle, S. Schroder, T. Geyer, G. Ekemb, and J. Nyobe-Yome, "Prediction of mechanical shaft failures due to pulsating torques of variable frequency drives," in *Proc. of the IEEE Energy Conversion Congress and Exposition, ECCE 2009*, San Jose, CA, USA, 2009, pp. 3469 – 3476.

[17] J. Song-Manguelle, J. Nyobe-Yome, and G. Ekemb, "Pulsating torques in pwm multi-megawatt drives for torsional analysis of large shafts," *IEEE Trans. Ind. Applicat.*, vol. 46, no. 1, pp. 130 – 138, 2010.

[18] J. W. Strutt and B. Rayleigh, *The Theory of Sound*. Dover Publications Inc., New York, 1945.

[19] L. E. Kinsler, A. R. Frey, A. B. Coppens, and J. V. Sanders, *Fundamentals of Acoustics*. John Wiley and Sons, New York, 1982.